Netherlands
organization for
applied scientific
research

TNO-report

FEL

TNO Physics and Electronics
Laboratory

TD 91-3918

P.O. Box 96864
2509 JG The Hague
Oude Waalsdorperweg 63
The Hague. The Netherlands

Fax +31 70 328 09 61
Phone +31 70 326 42 21

title

report no.   copy no.
FEL-91-B331

8

Estimation of the parameters used in the azimuth
compression

AD-A245 679

TDCK RAPPORTENCENTRALE
Frederikkazerne, Geb. 140
van den Burchlaan 31
Telefoon: 070-3166394/6395
Telefax : (31) 070-3166202
Postbus 90701
2509 LS Den Haag   *TDCK*

author(s):

ir. F.P.Ph.de Vries

date:

November 1991

**DTIC
ELECTE
FEB 0 4 1992
S   D
D**

classification

title	: unclassified
abstract	: unclassified
report text	: unclassified
appendix A	: unclassified

no. of copies	: 27
no. of pages	: 39 (incl. appendix, excl. RDP & Distr. list)
appendices	: 1

92-02795

TNO   92 2 03 1 57

report no.	:	FEL-91-B331
title	:	Estimation of the parameters used in the azimuth compression
author(s)	:	ir. F.P.Ph. de Vries
institute	:	TNO Physics and Electronics Laboratory
date	:	November 1991
NDRO no.	:	-
no. in pow '91	:	718.2

Research supervised by :

Research carried out by :

ABSTRACT (UNCLASSIFIED)

In azimuth processing of SAR data, the slant range histories of the targets are required. After range compression the maxima of the responses of a point target are on the so called range migration locus. For spaceborne SAR the locus traverses a number of range bins. This locus determines where to get the samples needed for the azimuth compression and the phase function which must be used. For satellite SAR the locus can be described by two parameters, the Doppler centroid f_{DC} and the frequency rate f_{DR}. These parameters can be estimated by using accurate spacecraft ancillary data and by utilizing the received radar data alone. This report describes the effects of errors in the parameters used by the processor and discusses algorithms to estimate the parameters. Examples of results from processing Seasat data are shown.

The report is one of a series for a SAR processor for the ERS-1 data, phase 2, precision processor. The work described was subsidized by the NIVR (NIVR, NRT nr, 2802 FE, SAR processor).

DTIC COPY INSPECTED 4

Accesion For	
NTIS CRA&I	☑
DTIC TAB	☐
Unannounced	☐
Justification	
By	
Distribution /	
Availability Codes	
Dist	Avail and / or Special
A-1	

SAMENVATTING (ONGERUBRICEERD)

Voor de azimut compressie van SAR data moet het verloop van de afstanden van de doelen tot de satelliet in de tijd bekend zijn. Na het comprimeren in range liggen de maxima van een puntdoel responsie op de zogenaamde range migratie locus. Voor satelliet SAR doorloopt deze locus een aantal afstandscellen. Deze locus bepaalt waar de bemonsteringen voor de azimut compressie liggen en de fase functie die gebruikt moet worden. Voor satelliet SAR zijn twee parameters voldoende om de locus te beschrijven. Deze parameters zijn, de Doppler centroide f_{DC} en de veranderingssnelheid van de Doppler frequentie f_{DR}. Deze parameters kunnen worden geschat uit nauwkeurige hulpdata van de satelliet en uit de ontvangen radardata zelf. Dit rapport beschrijft het effect van fouten in de parameters die door de processor gebruikt worden en bespreekt algoritmen voor het schatten van de parameters. Voorbeelden van resultaten verkregen met het processen van Seasat data worden getoond.

Het rapport is één uit een serie voor een precisie SAR processor voor ERS-1 data. Het beschreven werk is gesubsidieerd door NIVR (NIVR, NRT nr. 2802FE, SAR processor).

CONTENTS

1   INTRODUCTION

In the azimuth processing of the SAR data, the slant range histories of the targets are required. The changing slant range between the radar and the target as the radar moves past is $r(t)$. First, the azimuth samples used in azimuth compression have to be taken from different range gates in each pulse as dictated by $r(t)$. The slant range also determines the phase history

$$\phi(t) = (4\pi/\lambda)r(t) \qquad\qquad (1.1)$$

where λ is the radar wavelength.

The phase is used in generating the azimuth matched filter. Accurate determination of the functions is required. Errors in these functions degrade the image quality. The functions can be estimated by using accurate spacecraft ancillary data and by utilizing the radar echo data alone. Depending on the scene, with utilization of the raw radar data, greater accuracies can be achieved.

2 THE PHASE FUNCTION FOR A SPACEBORNE SAR

For spaceborne SAR's, the random motion of the spacecraft, which induce variations in the phase histories of the targets from those expected in a smooth flight path, is usually negligible. So, *motion compensation* (the techniques for removing the effects of the phase variations), is not required. It can be shown [Barber 85],[Li 85] that the expected phase history can be approximated by a function with two parameters c_1 and c_2

$$\phi(t) = c_0 + c_1 t + c_2 t^2 \qquad (1.2)$$

where $t = 0$ corresponds with the moment where the target is in the antenna boresight direction. The instantaneous Doppler frequency is given by

$$f(t) = -\frac{1}{2\pi} \frac{d\phi(t)}{dt} \qquad (1.3)$$

and

$$f(t) = f_{DC} + f_{DR} t \qquad (1.4)$$

The azimuth Doppler history is thus a linear chirp centred at f_{DC} having a Doppler rate f_{DR}. The two terms, f_{DC} and f_{DR}, will be referred to as the Doppler centroid and the Doppler frequency rate, respectively.

Thus, the range-migration curve $r(t)$ and the phase history curve $\phi(t)$ can be estimated by determining the two Doppler parameters.

In the sequel we use the following notations and simple relations

$$r(t) = a_0 + a_1 t + a_2 t^2 \tag{1.5}$$

$$c_1 = \frac{4\pi}{\lambda} a_1 \tag{1.6}$$

$$c_2 = \frac{4\pi}{\lambda} a_2 \tag{1.7}$$

and

$$f_{DC} = -\frac{2a_1}{\lambda} \tag{1.8}$$

$$f_{DR} = -\frac{4a_2}{\lambda} \tag{1.9}$$

3 THE EFFECT OF PHASE ERRORS

The accuracy requirements for the Doppler parameters are determined by the effects on image quality resulting from using erroneous parameters in the processor.

3.1 Doppler centroid f_{DC}

The response of a point target, in the range compressed domein, is a linear FM-signal

$$s_t(t) = a(t) \exp(j\phi(t)) \tag{1.10}$$

where $a(t)$ is caused by the antenna pattern. The antenna pattern is by construction a symmetric
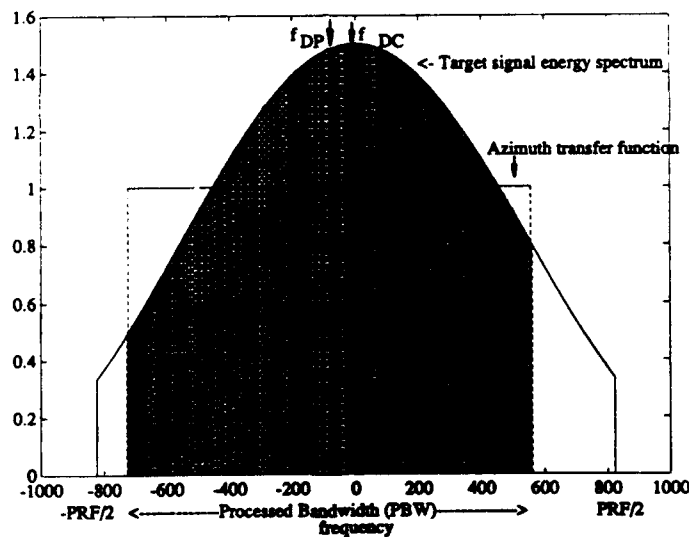

Figure 1.1: Frequency spectra of point target response and azimuth reference function

one. Assuming a target with no variations of backscatter as a function of azimuth angle, we find that $a(t)$ is a symmetric function. Thus the spectrum of the linear FM-pulse weighted by the symmetric function $a(t)$ is symmetric.
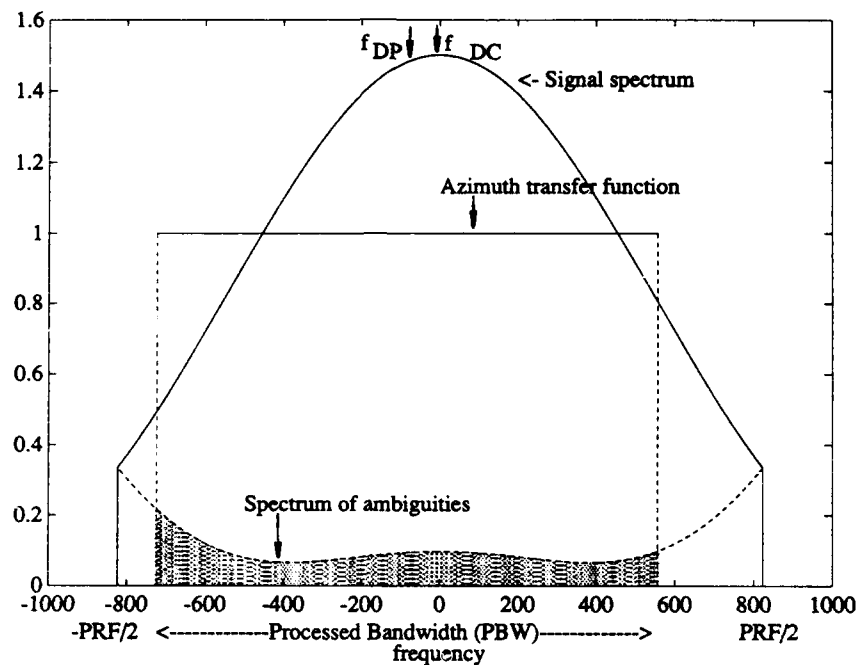
Figure 1.2:   Spectra of signal, ambiguities and azimuth reference function

The azimuth replica is a linear FM-pulse with constant amplitude so the azimuth transfer function is symmetric and flat having a fixed Processed Bandwidth (PBW). We get a maximum signal output when the reference Doppler centroid f_{DP} is equal to the signal centroid f_{DC}. By using an incorrect Doppler centroid we lose signal energy, as is evident from figure 1.1 (see also A12 in Appendix A). The white noise contribution to the correlator output does not depend on the centroid value f_{DP} used. Thus, Doppler centroid errors lead to a decrease in the signal-to-noise ratio (SNR).

The actual received radar signal is a stochastic signal $s(r,a)$, consisting of the superposition of point target responses, each having its own position (r_i,a_i), amplitude and phase. Note that we have replaced time t by azimuth a, which is proportional to t.

Now, consider the one-dimensional signal $s_r(a)=s(r,a)$, where r=constant. We get an estimate of the PSD of this signal by taking its Fourier transform $S_r(f)$ and determining $S_r(f)S_r^*(f)$. A better estimate is obtained by averaging a number of spectra adjacent in range.

Figure 1.3 shows three average image spectra (spectra of azimuth compressed Seasat data), corresponding with three different Doppler centroid values used by the processor. The spectrum

in the middle corresponds with the situation where the Doppler centroid value used by the processor is the Doppler centroid value of the signal ($f_{DP}=f_{DC}$). We see that the image spectrum is symmetric. The upper- and lower spectra correspond with Doppler centroid values $f_{DP} \neq f_{DC}$. The matched filter used by the processor has a frequency spectrum that does not centre on the maximum return of the antenna's azimuth power pattern which results in a asymmetric image spectrum.

The PRF is in the order of the frequency range traced out by the Doppler of the target during its traversal through the antenna main lobe. So there will be aliased energies in the processed bandwidth (PWB) from the ambiguities. The minimum amount of ambiguity energy is in the PBW when the processor Doppler centroid f_{DP} equals the correct Doppler centroid f_{DC}. Thus Doppler centroid errors lead to a decrease in the signal-to-azimuth ambiguity level ratio, as is evident from figure 1.2. The azimuth ambiguity and a definition of a signal-to-ambiguity ratio (SALR) is discussed in [Tomiyasu 80].

In [Li 85] (see also [Curlander 82] the nominal orbital and radar system parameters for the Seasat SAR have been used to generate curves for f_{DC} and f_{DR} at the radar boresight as a function of the true anomaly of the orbit for the cases with no spacecraft attitude errors and with 1° error in yaw and 1° error in pitch. These attitude errors can cause Doppler centroid shifts of more than 1000Hz (the PRF is ~ 1647Hz). Also evaluated and plotted were the losses in SNR and SALR as a function of the Doppler centroid error. The plots show that the SALR deteriorates much faster, as a function of Doppler centroid error, than the SNR. For losses in SALR and SNR both less than 3db, the Doppler centroid error must be less than ~150Hz, which corresponds with a spacecraft attitude uncertainty of less than ~0.2°. For the Seasat experiment, the attitude is generally determined to better than ~0.1°. There are occasions, however, when, the attitude is not known to better than ~0.7° due to malfunctioning of the attitude determination system, the attitude is not known to better than ~0.7°. In these cases use of the resulting erroneous estimates causes significant losses in SNR and SALR. Furthermore, there are applications using SAR data that require very accurate estimates of f_{DC}. These accurate estimates can be obtained using the radar echo data themselves.

In Appendix A, we have shown that the point target response is shifted in time (azimuth) and range from its correct position when using an incorrect Doppler centroid value.

The shift in the azimuth dimension is

$$\tau = \frac{a_{1r} - a_{1t}}{2a_{2t}} = \frac{f_{DP} - f_{DC}}{f_{DR}} \qquad (1.11)$$

and the shift in the range dimension is

$$\rho = \frac{a_{1r} - a_{1t}}{2}\tau = \frac{-\lambda}{2f_{DR}} \frac{(f_{DP} + f_{DC})}{2}(f_{DP} - f_{DC}) \qquad (1.12)$$

The shift in the azimuth dimension is illustrated by Figure 1.4. Shown are 8 images of the Seasat scene containing the Goldstone antenna. For each image a different processor Doppler centroid value f_{DP} was used. The frequency values between two adjacent images differ by 17.0 Hz. For each image, range goes from left to right and the azimuth is in the vertical direction.

3.2 Doppler frequency rate f_{DR}

Consider a point target which at $t=0$ is in the antenna boresight direction. To image the target we can use any interval of the target locus within the Processed Bandwidth (PBW), e.g. the interval with length T_a and centre τ (see Figure 1.5). The azimuth resolution is determined by the aperture (T_a). If an incorrect Doppler frequency rate is used, the maximum target response will occur at azimuth (time) and range not corresponding with the target's azimuth and time. This is the case because the (wrong) reference locus will approximate the target locus best at a part different from the one sketched in Figure 1.5. The reference locus does not, however, completely coincide with the target locus. So (slightly) wrong data is taken and a (slightly)wrong phase reference function is used. The resulting point target image is shifted from the true position, the response is broadened and the peak gain is reduced. These effects are functions of the cumulative phase errors. The shift of the point target response depends on τ (the azimuth centre value of the processing interval).

The effect of an error in the Doppler frequency rate in a n-look SAR processor is that each target will appear as n separate targets in the image.

The shift in time is (see [Li 85])

$$\delta t = \frac{f_{DR} - f_{rP}}{f_{rP}} \tau = \frac{\delta f_{DR}}{f_{rP}} \tau \qquad (1.13)$$

where f_{DR} is the correct Doppler frequency rate, f_{rP} the frequency rate used by the processor , δf_{DR} the rate error and τ the look's centre time.

For 4-looks, we find a time shift of the two images corresponding with the extreme looks LL and RR (see figure 1.5) of

$$\delta t = \frac{\delta f_{DR}}{f_{rP}} \frac{3T_{\alpha}}{4} \qquad (1.14)$$

where T_a is the maximum available azimuth integration time.

Using typical Seasat values, we get for the displacement between two look-images $\delta x = v \delta t$

$$\delta x - 25 \, \delta f_{DR} \quad m \qquad (1.15)$$

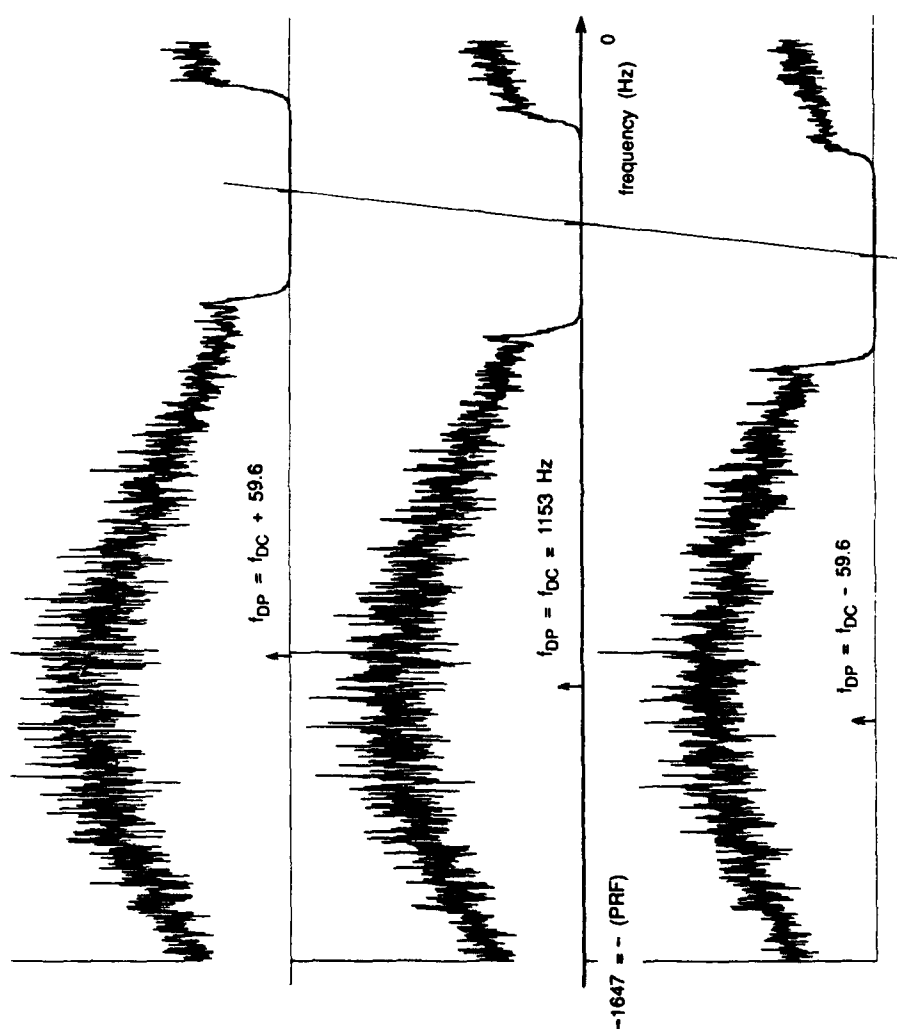Figure 1.3: Average image spectra for different Doppler centroid values f_{DP}, from top to bottom $f_{DP} = f_{DC} + 59.6$, $f_{DP} = f_{DC}$ and $f_{DP} = f_{DC} - 59.6$
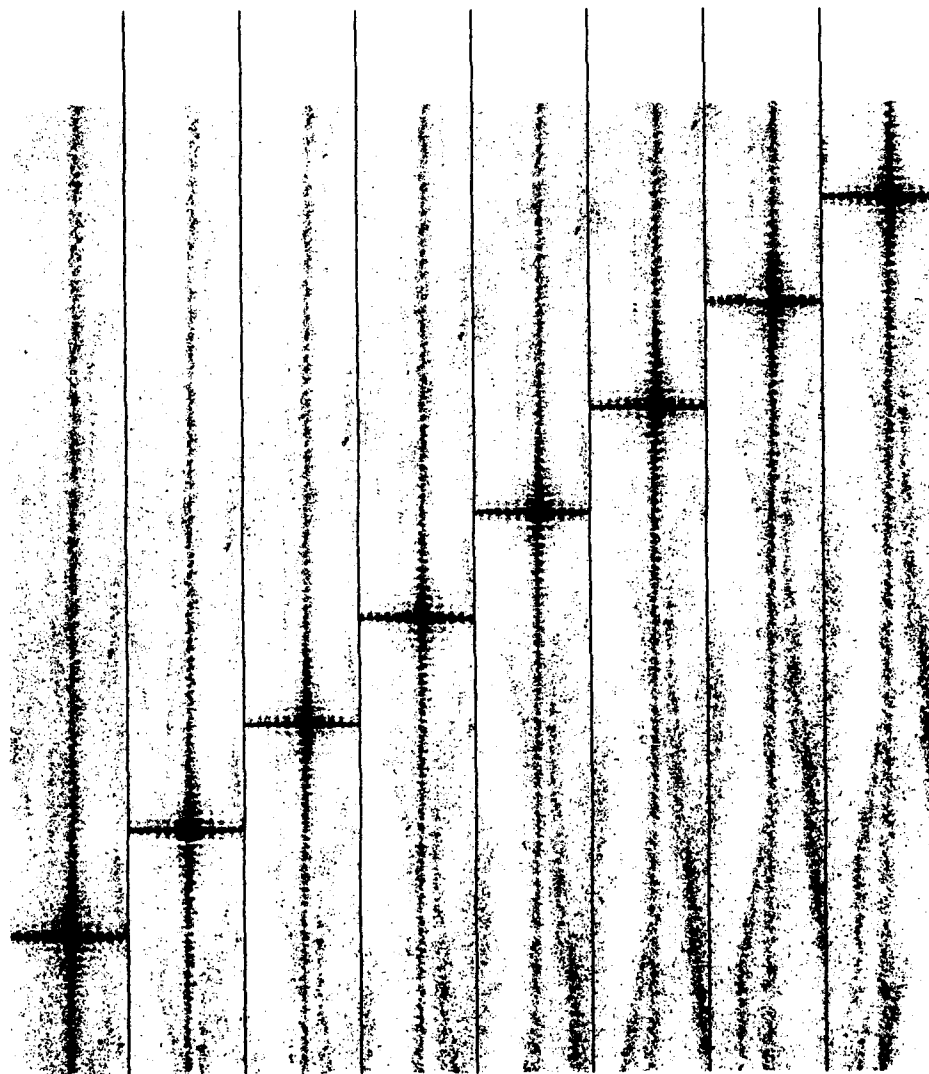
Figure 1.4: Images of the Seasat data containing the Goldstone antenna for 8 different Doppler centroid values f_{DP}. Frequency difference between two neighbour images is 17.0 Hz. Range in horizontal and azimuth in vertical direction.
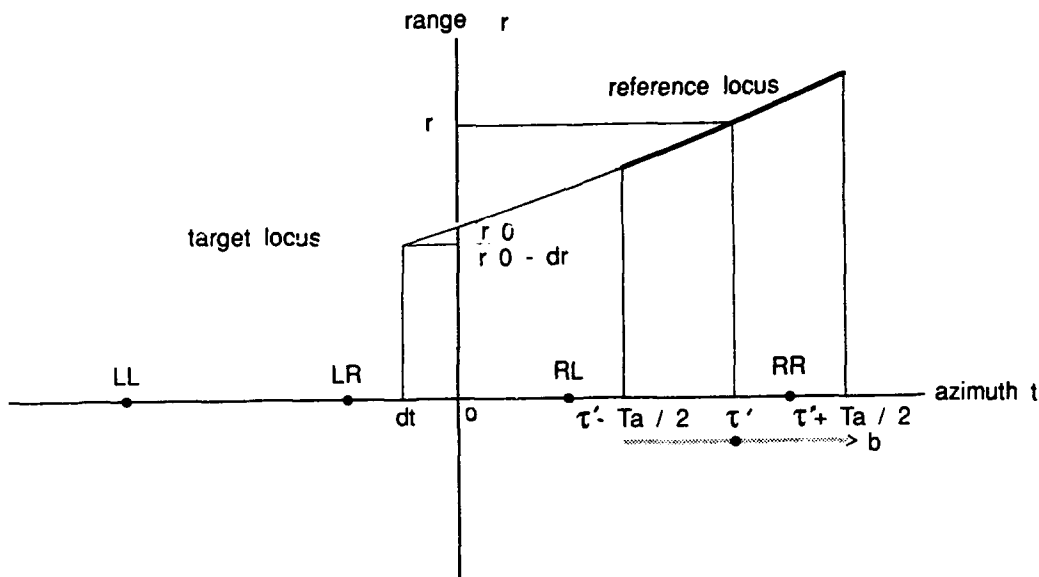
Figure 1.5: Position of reference locus ($t = \tau$) and target locus ($t = 0$). Indicated are centre times of reference loci when using 4-looks (LL, LR, RL and RR).

where $T_a = 2.48$ sec, v ~ 7000m/sec and $f_{rP} \approx f_{DR} \approx 530$Hz/sec.

The resolution of the four look Seasat image is ~25m. If we constrain the image displacement to less than 8m than $\delta f_{DR} < 0.3$ Hz/sec. The corresponding cumulative phase error in each subaperture is ~5°. This phase error generates acceptable degradation in each look's point target response.

The Doppler rate f_{DR} is not as sensitive to the spacecraft attitude fluctuations [Curlander 82] as the Doppler centroid. An analysis of the error sources in the estimation of f_{DR} using this technique indicates that uncertainty in $\vec{v}_s$, the velocity of the satellite, is the major f_{DR} estimation error source. It has been determined that for Seasat a satisfactory value for f_{DR} is within 0.75Hz/sec of the true f_{DR}. This accuracy level can be obtained if $\vec{v}_s$ is known to better than 0.5m/sec in each component. Thus using the ancillary data approach may provide an

adequate estimate for f_{DR}. For future *real time* SAR processors, when only approximate estimates of the ancillary spacecraft data are available, the expectation is that such accuracies will be difficult to obtain. Use of an autofocus method, therefore, can be advantageous.

4   DOPPLER PARAMETER DETERMINATION TECHNIQUES

Report [Otten 89] presents a study of available literature on phase error reduction techniques, supplemented by comments of general nature. For satellite SAR the phase history can be approximated by a function with the two Doppler parameters: the Doppler centroid f_{DC} and the Doppler rate f_{DR}. The two techniques, to estimate these parameters, described in this report achieve accuracies which can exceed the system performance requirements. The methods to estimate the two Doppler parameters f_{DC} and f_{DR} are referred to as "clutterlock" and "autofocus" respectively. The methods are computationally more demanding than the parameter estimation based on accurate spacecraft ancillary data. So, when the potentially more accurate estimates are not needed, we use the ancillary data. Moreover, both the clutterlock and autofocus methods need initial estimates. These initial estimates are provided by the values determined from the ancillary data or, in cases where such data are not available, by estimates from simpler implementations of the clutterlock and autofocus techniques.

4.1   Doppler parameter estimation derived from spacecraft ancillary data

Figure 1.6 shows the imaging geometry involved for a spacecraft SAR. The range from satellite to
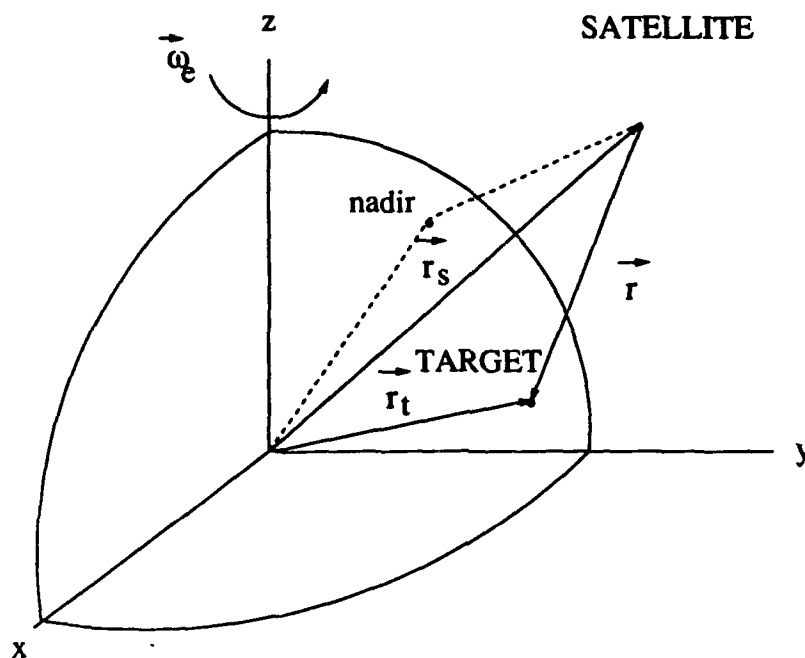
Figure 1.6:   Geometry of relative position between sensor and point target

target is given by

$$\vec{r}(t) = \vec{r}_T(t) - \vec{r}_S(t) \qquad (1.16)$$

where $\vec{r}_T(t)$ refers to the position vector of the target on the Earth's surface and $\vec{r}_S(t)$ refers to the position vector for the satellite.

The target's motion can be modeled as a point on the surface of a rigidly rotating Earth, so

$$\vec{r}(t) \approx \vec{r}_T(0) + \vec{v}_T(0)t + \frac{1}{2} \vec{a}_T(0)t^2 \qquad (1.17)$$

where $\vec{v}_T(0) = \vec{\omega}_e \times \vec{r}_T(0)$, $\vec{\omega}_e$ is the Earth's angular velocity vector and $\vec{a}_T(0)$ is the acceleration vector of the target.

For small t, the satellite motion is modeled as

$$\vec{r}_S(t) \approx \vec{r}_S(0) + \vec{v}_S(0)t + \frac{1}{2}\ \vec{a}_S(0)t^2 \tag{1.18}$$

where $\vec{v}_S(0)$ and $\vec{a}_S(0)$ are the velocity and acceleration vectors of the satellite.

Substituting 1.17 and 1.18 into 1.16

$$\vec{r}(t) = \vec{r}(0) + \vec{v}(0)t - \frac{1}{2}\ \vec{a}(0)t^2 \tag{1.19}$$

where

$$\vec{r}(0) = \vec{r}_T(0) - \vec{r}_s(0)$$

$$\vec{v}(0) = \vec{v}_T(0) - \vec{v}_s(0)$$

$$\vec{a}(0) = \vec{a}_T(0) - \vec{a}_s(0)$$

Inserting 1.19 into $r(t) = \sqrt{\vec{r}(t) \cdot \vec{r}(t)}$ and retaining terms to t^2 we get

$$r(t) = r(0)\sqrt{1 + \frac{2\{\vec{r}(0) \cdot \vec{v}(0)\}t + [v^2(0) - \vec{r}(0) \cdot \vec{a}(0)]t^2}{r^2(0)}}$$

the second square root term is small compared to 1, so we can use

$$\sqrt{1 + x} \approx + \frac{x}{2}$$

We find

$$r(t) \approx r(0) + \frac{\vec{r}(0) \cdot \vec{\upsilon}(0)}{r(0)} t + \frac{\upsilon^2(0) - \vec{r}(0) \cdot \vec{a}(0)}{2r(0)} t^2 \qquad (1.20)$$

Using 1.5 through 1.9 we get

$$f_{DC} = -\frac{2a_1}{\lambda} = -\frac{2}{\lambda} \frac{\vec{r}(0) \cdot \vec{\upsilon}(0)}{r(0)} \qquad (1.21)$$

$$f_{DR} = -\frac{4a_2}{\lambda} = -\frac{2}{\lambda} \frac{\upsilon^2(0) - \vec{r}(0) \cdot \vec{a}(0)}{r(0)} \qquad (1.22)$$

The spacecraft position $\vec{r}_S(0)$ and velocity $\vec{\upsilon}_S(0)$ are typically known from the orbit tracking data and the acceleration is easily determined assuming negligible drag (i.e. purely gravitational acceleration).

The target location $\vec{r}_T(0)$ is found by solving the vector equation: $\vec{r}_T(0) = \vec{r}_S(0) + r(0) \vec{b}_a$ assuming some earth model where $\vec{b}_a$ is the boresight unit vector and r(0) is the slant range from satellite to target. The position of the target on the earth's model and the rotational velocity vector $\vec{\omega}_e$ determine the velocity vector $\vec{\upsilon}_T(0)$. Since both the satellite and target postion, velocity and acceleration are known, the Doppler parameters and therefore the range migration locus and azimuth reference function can be determined. Since for a typical SAR the antenna is rigidly mounted to the satellite platform, the attitude variation is directly translated to the boresight of the radar. Thus $\vec{b}_a$ must be adjusted for the attitude of the satellite. The accuracy of this vector is therefore directly dependent on the uncertainty in the spacecraft attitude determination system. As mentioned before the ancillary data approach for determination of f_{DC} is unsatisfactory whereas it may provide an adequate estimate for f_{DR}.

4.2 Doppler centroid determination, CLUTTERLOCK

The technique to determine the Doppler centroid from the radar echo data is based on the fact that the radar echo data consists of the superposition of a large number of scatterers. A point target response in the azimuth direction is a linear FM-signal, centred on the Doppler centroid, modulated by the antenna pattern. This antenna pattern is by design symmetric about its peak. So,

if in a scene a very dominant point target was present we could find the frequency which corresponds with the peak response.In reality the radar signal consists of a superposition of a large number of scatterers. The resulting signal will be a sample function from a random process. Now, assume a target area which has a homogeneous scatter density, and that the scatterers show no variations of backscatter cross sections as a function of azimuth angle. Then, the power spectral density (PSD) of the azimuth spectra has the shape of the antenna power pattern and again the frequency corresponding with the peak density is the Doppler centroid. The technique used to estimate the Doppler centroid consists of estimating the PSD by computing the periodogram of an azimuth line (that is at constant range). To obtain statistically consistent periodogram spectra a number of periodograms from adjacent ranges are averaged. The number must not be too large since f_{DC} is a function of range. In Figure 1.7 we have indicated the domains were the PSD can be determined.

PROCESSING

ENCODING   RANGE   AZIMUTH

$$\sigma_c(a,r) \rightarrow \boxed{H_e(f_a - f_{DC}, f_r)} \rightarrow \bigcirc\!\!\Sigma \rightarrow \boxed{H_r(f_r)} \rightarrow \boxed{H_a(f_a - f_{DP}, f_r)} \rightarrow g(a,r)$$

$$n(a,r)$$

① ② ③
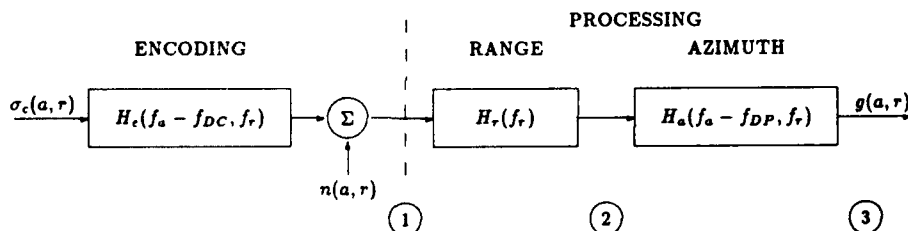
Figure 1.7:   SAR encoding and processing; 1, 2 and 3 indicate domains from which the data can be used for estimation of the Doppler centroid.

Two problems have to be treated in the SAR modelling. One is to relate the scene reflectivity and the complex output image. Secondly, a model for the radar scene is required. These problems have been treated, extensive references can be found in [Madsen 89]. In Figure 1.7, $\sigma_c(a,r)$ is the complex radar cross section $|\sigma_c(a,r)|^2 = \sigma(a,r)$ in azimuth and slant range coordinates, f_a and f_r are frequencies in the azimuth and range dimensions, H_e represents the encoding of the scene, $n(a,r)$ indicates thermal noise, H_r is the range compression and H_a is the azimuth compression. For the PSD estimation we use windows. There will be a lot of target responses that are only partially covered by the window. The influence of this fact on the estimation quality is more severe as a target response effectively covers a large area. The most confined response occurs in the final domain, the image domain (point 3). So the best results are obtained by estimation based

on the range- and azimuth compressed data, which, however, requires that f_{DP} is taken into consideration, leading to an iteration procedure. The main advantage of using the raw data, point 1, is that the estimation procedure will not depend on the processor setting f_{DP}. Estimation, using data from this domain is therefore faster than by utilization of image data and can be used in realtime processing. The raw data can also serve for an initial estimate. Since we are concerned with the precision processor, we have chosen for the estimation of the Doppler centroid f_{DP}, based on the complex image data (point 3).

The implemented Doppler centroid estimation method is the so-called Δ E-method. The Δ E-method assumes a PSD showing symmetry about the true Doppler centroid. If the processor centroid f_{DP}, equals this true centroid we have this symmetry. Then, computing the energy E_l in the interval at the lefthand side of f_{DP}, and the energy E_r in the righthand interval, we find $E_r = E_l$. If an incorrect processor centroid value is used, the energies will differ $\Delta E = \Delta E_{rel} = \frac{E_r - E_l}{E_r + E_l} \neq 0$. Using a number of different processor centroid values we find a curve which is highly linear. By fitting a linear function of frequency to the computed ΔE values we can determine the intercept with the f_{DP} axis (i.e. the frequency value where $\Delta E = 0$). This frequency value $\hat{f}_{DC}$ is the estimate of the Doppler centroid f_{DC}.

Figure 1.8 shows the blockdiagram of the Doppler centroid line (the Doppler centroid is a function of range) estimator. The clutterlock algorithm, called the Δ E-method operates as follows:

1. Based on a quick look processing, a portion of the raw SAR data to be processed into an image is selected. The portion is divided into intervals, the data in an interval centred on range r is used to estimate the Doppler centroid $\hat{f}_{DC}(r)$. Over the relatively small area used to estimate the centroid line, the theoretical variation of the Doppler centroid as a function of range is approximately linear. An interval must be large enough to be able to perform statistical averaging to get stable estimates but not too large since the Doppler centroid may be considered constant only for short range intervals. We have used an image covering an area ≈ 16km by 8km (1024range × 2048 azimuth samples). The image is divided into intervals of 64 range samples and 2048 azimuth samples.

2. The raw SAR data area is range compressed and corner turned yielding a data area of 1024 R × 2048 A samples. It has been found necessary to use a high degree of interpolation (8 new samples per old one) to reduce the modulation effect on the spectrum caused by the range sampling grid. Thus the input to the azimuth compression stage consists of (64 × 8) R × 2048 A samples.
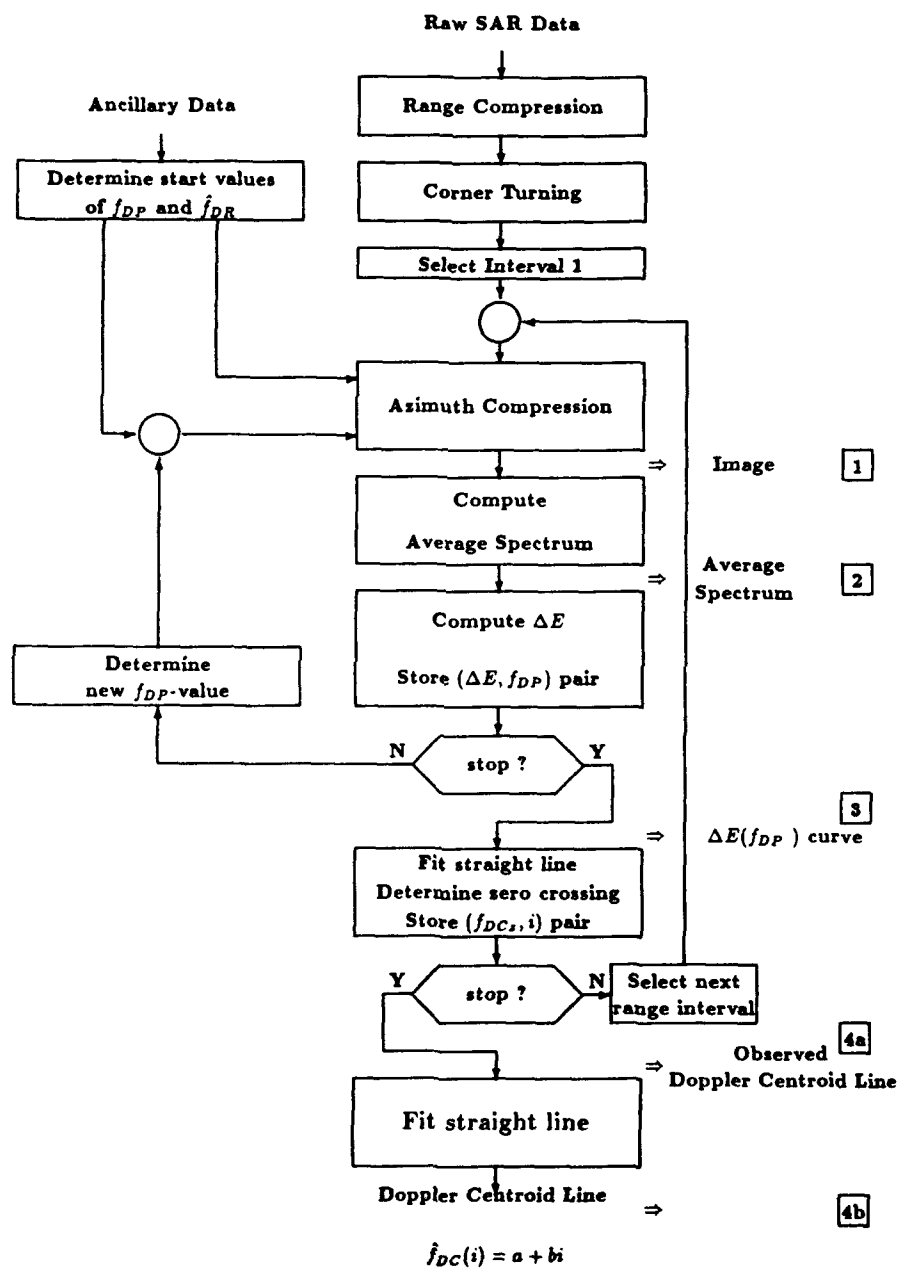
3. Based on the ancillary data, initial estimates of the Doppler rate f_{DR} and the Doppler centroid f_{DC} are determined.

4. To determine the range dependence of f_{DC}, the range compressed data are divided into 16 range intervals (each containing 64×8 range lines, where 8 is due to the interpolation). An image of 2048 azimuth samples is obtained using the full available aperture of 4096 azimuth reference samples. For each interval the parameters used are f_{DR} obtained in step 3 and one of 16 values of f_{DP}. An initial value of f_{DP} is obtained in step 3. The 16 values f_{DP} are chosen to be equidistant and symmetrically distributed around the f_{DC} value obtained in step 3, the increment is 8.5Hz.

5. Azimuth frequency spectra are generated by obtaining the periodograms of the complex imagery in the azimuth direction. The periodograms are averaged to give a higher spectral fidelity. An example of spectra for different processor values f_{DP} (point 2 in Figure 1.8) is shown in Figure 1.3.

6. The energy difference

$$\Delta E = \frac{E_r - E_l}{E_r + E_l}$$

is computed and the pair $\Delta E(f_{DP})$, f_{DP} is stored. An example of a ΔE versus f_{DP} curve (point 3 in Figure 1.8) is shown in Figure 1.9.

7. A straight line is fitted to the 16 pairs $(\Delta E, f_{DP})$, and the f_{DP} value corresponding to $\Delta E = 0$ $(f_{DC\ i})$ is determined. The pair $(f_{DC\ i}, i)$ is stored.

8. The steps 4 through 7 are repeated for all 16 range intervals. To the observed (f_{DC_i}, i) data, a linear function is fitted. The line so obtained is the Doppler line. An example of the Doppler centroid estimates and a linear fit for the 16 range intervals is shown in Figure 1.10.

To get an estimate of the error in each determined Doppler centroid value the approach of [Li 85] is followed. As mentioned before, over the relatively small area of the scene of $\approx$ 16km by 8km, the theoretical variation of the Doppler centroid as a function of range is approximately linear (typical nonlinear effects are estimated to be 0.2Hz in the reference). So the root-mean-square deviation

Raw SAR Data

Ancillary Data

Range Compression

Determine start values
of f_{DP} and $\hat{f}_{DR}$

Corner Turning

Select Interval 1

Azimuth Compression

$\Rightarrow$ Image $\boxed{1}$

Compute

Average Spectrum

$\Rightarrow$ Average
Spectrum $\boxed{2}$

Compute ΔE

Store $(\Delta E, f_{DP})$ pair

Determine
new f_{DP}-value

N stop ? Y

$\Rightarrow$ $\Delta E(f_{DP})$ curve $\boxed{3}$

Fit straight line
Determine sero crossing
Store (f_{DC_s}, i) pair

Y stop ? N Select next
range interval

$\Rightarrow$ Observed $\boxed{4a}$
Doppler Centroid Line

Fit straight line

Doppler Centroid Line $\Rightarrow$ $\boxed{4b}$

$$\hat{f}_{DC}(i) = a + bi$$

Figure 1.8:   Block diagram of Doppler centroid estimation algorithm (ΔE method)
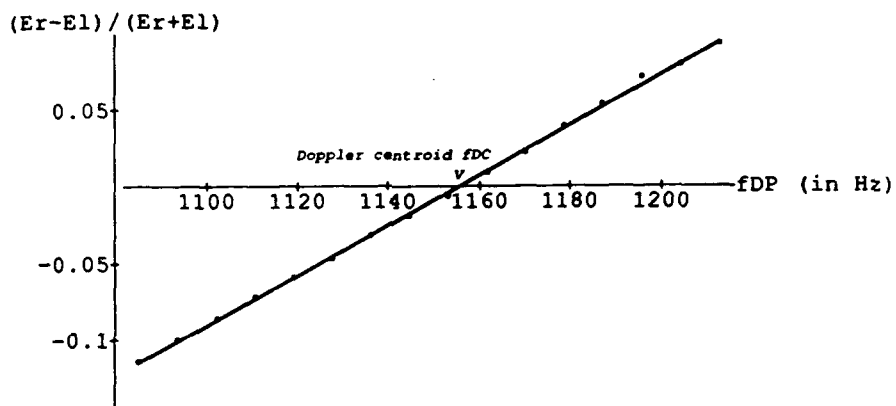
Figure 1.9:   Plot of energy difference against several values of processor Doppler centroid f_{DP}. Estimated centroid is f_{DC}.

from the regression line (the Doppler centroid line from step 8) is taken as a measure of accuracy. The value obtained in step 8 is 16.8Hz.

In [Madsen 86], the standard deviation of the estimator $\hat{f}_{DC}$ is calculated under the assumption that the scene is quasi stationary, that is, $\sigma_0(\vec{r}\ )$, the average backscatter coefficient is slowly varying compared with the system impulse response. One of the most important results is that the variance of the estimator is proportional to the scene contrast, SC, defined as

$$SC = \frac{<\sigma^0(\vec{r})^2>}{<\sigma^0(\vec{r})>^2}$$

where < > indicates spatial averaging.

Estimation results in [Li 85] and [Curlander 82] show that the estimation accuracy is highly dependent on scene type, e.g. urban, desert, mountain, etc. and that successful implementation requires an algorithm capable of automated detection of estimation errors that result from unsatisfactory selection of a test area.

Scenes that exhibit an asymmetric azimuth reflectivity will produce a degraded Doppler centroid estimate. The scene types that exhibit this directional reflectivity characteristic generally have a very rough surface such as mountain or urban areas. Conversely a flat surface such as ocean or desert produce highly precise estimates. Test results in [Curlander 82] show that the estimate uncertainty for ocean is between 1-3Hz (1 σ) while that for urban areas is 16-24*Hz* (1 σ).
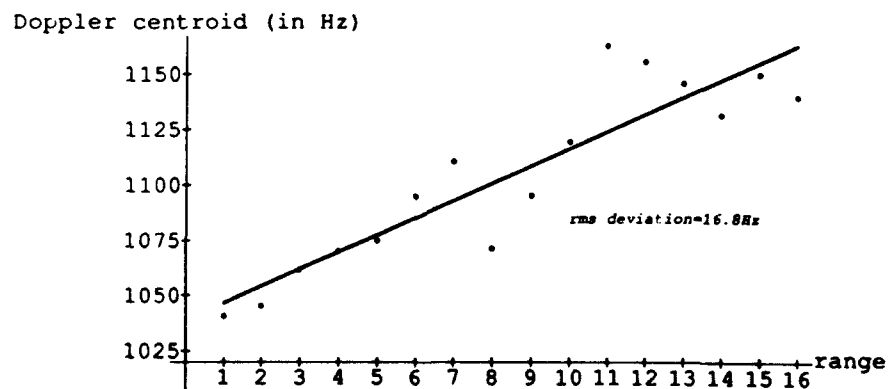
Doppler centroid (in Hz)

rms deviation=16.8Hz

range

Figure 1.10: Doppler centroid estimates and linear fit for 16 range intervals. Δ E-method.

4.3 Doppler centroid estimation, time domain estimation

An alternative way of finding the Doppler centroid is by using the Fourier relation between the PSD and the autocorrelation. [Madsen 89] describes two methods, the correlation Doppler estimator (CDE) based on a linear estimator of the autocorrelation function and the sign-Doppler estimator (SDE) based on a nonlinear estimator of the autocorrelation function. The SDE-method derives the autocorrelation properties of an assumed circular symmetric Gaussian process by analyzing the sign alone. This means first of all that the majority of calculations involved in the estimation are extremely simple (that is, sign comparisons) and therefore the algorithm is well suited to real-time implementation. Secondly, the estimator does not give more weight to strong targets which makes it less sensitive to strongly varying scenes.

The conclusions of [Madsen 89] are that the time domain algorithms are efficient with respect to requirements on calculations and memory and hence well suited to real-time systems where the Doppler estimation is based on raw data. For off-line processors where the Doppler estimation is performed on the image data, the ΔE estimator and the CDE algorithm give similar performance. However, when it comes to nonhomogeneous scenes, it is found that the nonlinear SDE algorithm gives superior performance.

We have implemented both the CDE and the SDE algorithms. Test on a small sample of data showed results almost equal to the ones obtained with the ΔE-method. To verify the claim of the SDE-algorithm with respect to nonhomogeneous scenes a lot of additional work needs to be done.

4.4 Doppler frequency rate determination, AUTOFOCUS

Sar data, in the azimuth dimension, have the property that from any subaperture of the synthetic aperture an image can be computed of the same target. The images will be of the same target except that the resolution will be reduced because only a part of the full aperture (and hence from the full Doppler induced FM bandwidth) is taken. Use of an incorrect Doppler frequency rate value f_{rp} in the processor causes the defocus of the image and a shift in the azimuth direction (also called map-drift). This shift depends on the position of the subaperture in the synthetic aperture (Section 1.3.2). The autofocus method is based on this shift property. The aperture is divided into two subapertures and an image is formed from each subaperture based on the processor Doppler frequency rate f_{rp}.

The two images are cross-correlated to detect the registration error. Based on the detected error a new processor parameter is computed. This iteration procedure is stopped when the two images become focussed, that is show an acceptable shift with respect to each other. This map-drift

method is a method specific to measuring a quadratic phase error. In general, n subapertures are required to measure an nth-order phase error polynomial [Brown 88].

Figure 1.11 shows the block diagram of the Doppler frequency rate line (the Doppler frequency rate is a function of range) estimator. The estimator is tested with Seasat scene data from an area near the Goldstone tracking station. The scene contains several bright point-like images of corner reflectors that were deployed for calibration purposes. The autofocus algorithm operates as follows:

1. Based on a quick look processing, a portion of the raw SAR data to be processed into an image is selected. The portion is divided into range intervals, the data in an interval i is used to estimate the average cross-correlation function $R_{LR}(k,i)$. Over the relatively small area used to estimate the correlation function, the Doppler frequency rate f_{DR} (which is a function of range, formula 1.22, is considered constant $f_{DR}(r) \equiv f_{DR}(i)$. Since the processor rate value $f_{rP}(i)$ is taken constant in the ith range interval, the map drift value of each line of the interval is approximately constant. The image used covers an area ≈ 37 km by 8 km (2048 range $\times$ 2048 azimuth samples). The image is divided into 128 intervals of 16 lines of 2048 azimuth samples.

2. The raw SAR data area is range compressed, with 1 $\times$ interpolation and corner turned yielding a data area of 2048 R $\times$ 2048 A complex samples.

3. Based on the ancillary data, initial estimates of the Doppler centroid f_{DC} and the Doppler frequency rate f_{DR} are determined.

4. A range interval i is azimuth compressed into an L-look and an R-look image of 16 $\times$ 2048 samples. The complete available spectral band of 4096 azimuth samples is used. The band is divided into two non-overlapping subbands of 2048 azimuth samples. The processor parameters used are f_{DC} as obtained in step 3 and the interval Doppler frequency rate value $f_{rP}(i) = A + Bi$. An initial value of f_{rP} is, $f_{rP}(i) \equiv f_{rP}$ ($A=f_{DR}$ as obtained in step 3 and $B=0$). Figure 1.12 shows an example of look images obtained by using three different processor values for the Doppler frequency rate. Here the range interval consists of 80 samples. For each line the same f_{DP} value (Doppler centroid value used by the processor) is taken.

5. The L-look and R-look images are line by line cross-correlated and the obtained 16 cross-correlation functions are averaged yielding $R_{LR}(k,i)$. Typical average cross-correlation functions $R_{LR}(k)$ for different values of the Doppler frequency rate used by the processor are shown by Figure 1.13. Due to the blurring of the look-images when incorrect f_{DR} values are used, the cross-correlation peak broadens.

6. The location $kmax(i)$ of the peak of the average cross-correlation function $R_{LR}(k,i)$ (i.e. the shift between both images) is determined. The quality of the lag estimate deteriorates as the error in the processor Doppler frequency rate increases due to the broadening of the cross-correlation peak.

Ancillary Data　　　　**Raw SAR Data**

Determine start values
of $\hat{f}_{DR}$ and $\hat{f}_{DC}$

Range Compression

$f_{rP}(i) = A + Bi$　$f_{DP} \equiv \hat{f}_{DC}$
$A = \hat{f}_{DR}$; $B = 0$
Initial (A, B) pair

Corner Turning

Select Range Interval 1

f_{rP}　f_{DP}

Azimuth Compression
L-look

1a
$\Rightarrow$ L-look
Image

Azimuth Compression
R-look

1b
$\Rightarrow$ R-look
Image

Compute Average Cross-
correlation Function
of the Look Images
Store $R_{LR}(k, i)$

2
$\Rightarrow$ Average
Cross-correlation
Function $R_{LR}(k, i)$

next f_{rP}-value
$f_{rP} = A + Bi$

Determine Location $kmax(i)$
of the peak of the
cross-correlation function
Store $(kmax, i)$ pair

N ⟨Last Interval ?⟩ Y

3a
$\Rightarrow$ Observed Lag Line

Fit straight line
$a + bi$
to the $kmax(i)$ curve

3b
$\Rightarrow$ Estimated Lag Line

Determine next
(A, B) pair

N ⟨$\Sigma kmax(i)^2 < \epsilon$?⟩ Y

Doppler Rate Line
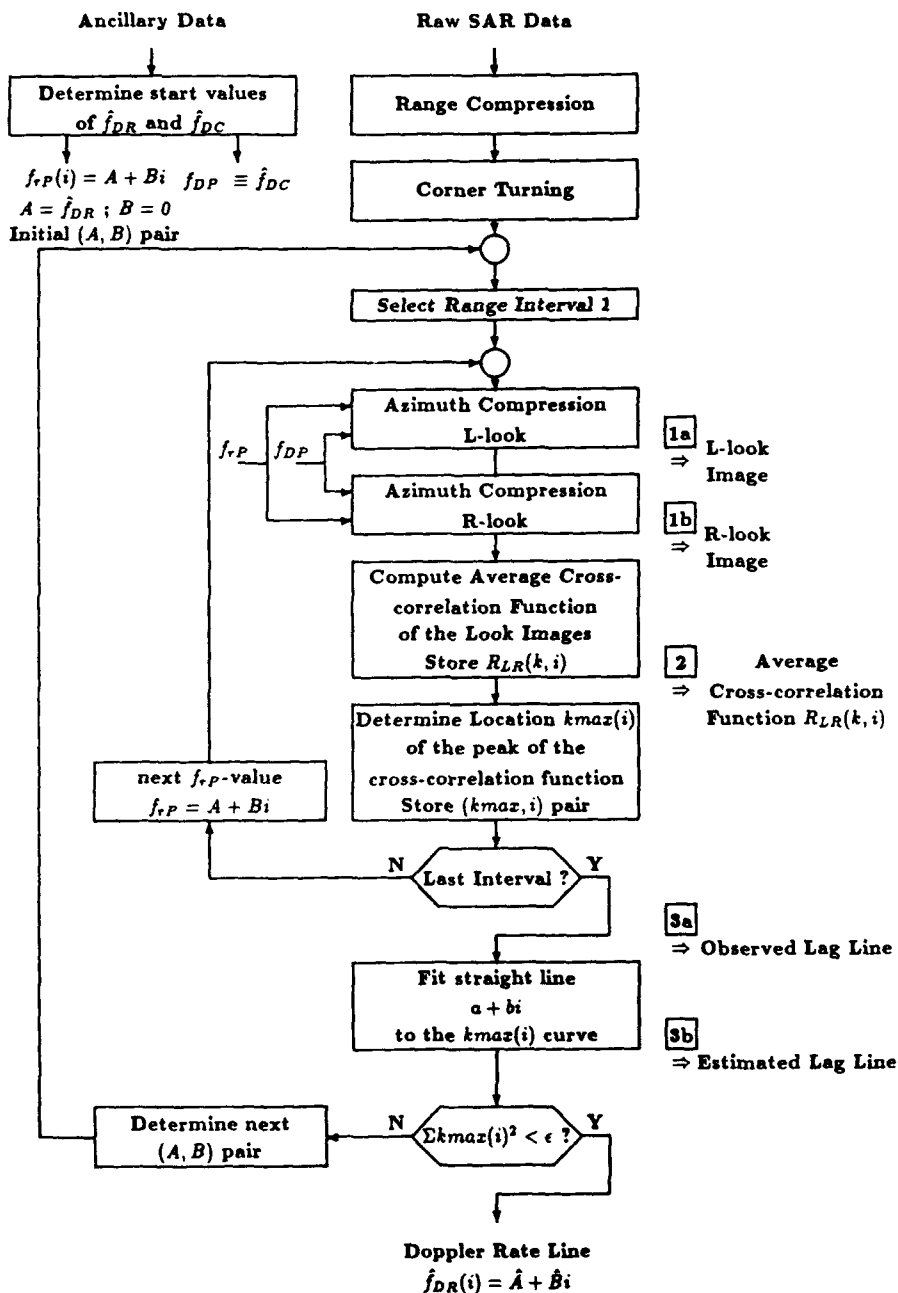$\hat{f}_{DR}(i) = \hat{A} + \hat{B}i$

Figure 1.11:　Block diagram of Doppler rate estimation algorithm (AUTOFOCUS)

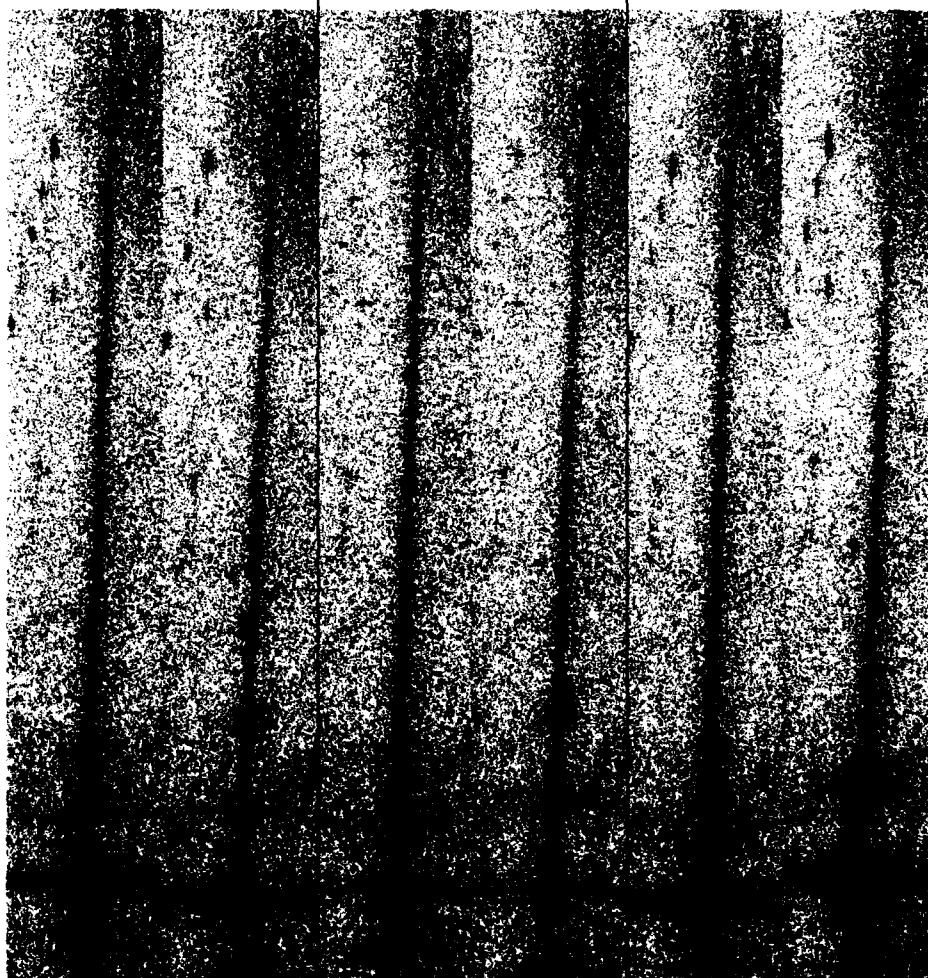Figure 1.12: Goldstone look-images for different processor Doppler frequency rates f_{rp}. From left to right: f_{rp}=502Hz/sec, f_{rp}=f_{DC}=516Hz/sec (focussed) , f_{rp}=536Hz/sec. Range in horizontal and azimuth in vertical direction.
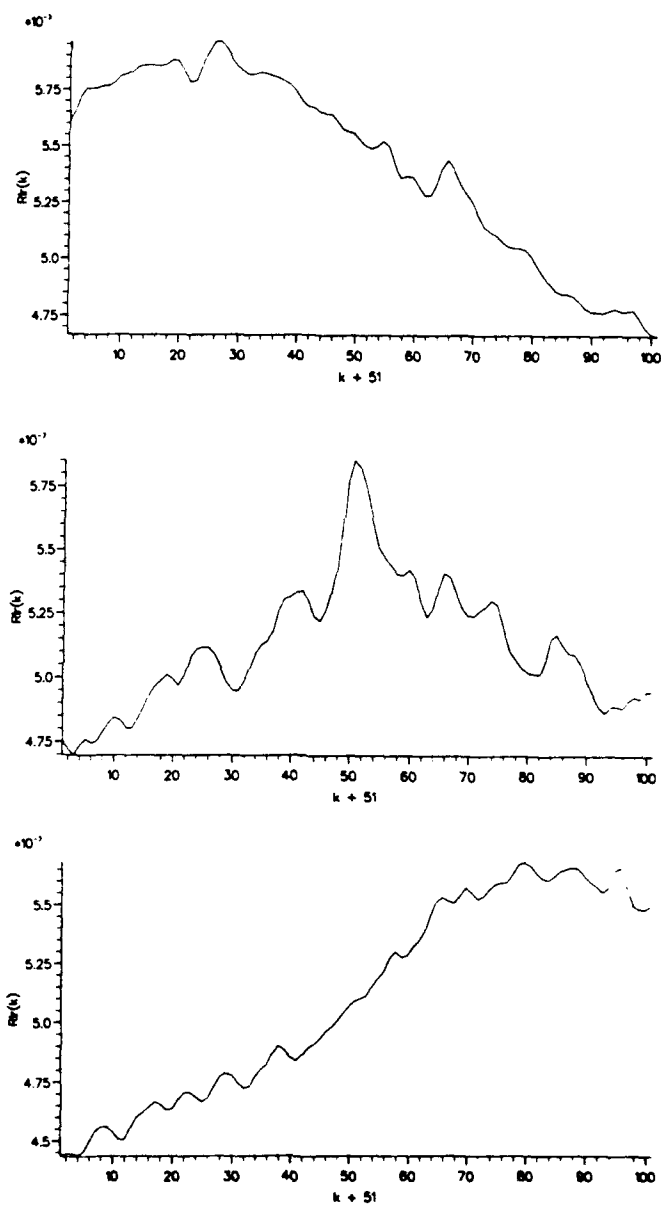
Figure 1.13: Typical average cross-correlation functions $R_{LR}(k)$ for different processor Doppler frequency rates f_{rp}. From top to bottom f_{rp}=506Hz/sec , $f_{rp}=f_{DR}$=516Hz/sec (focussed), f_{rp}=526Hz/sec. Note: due to the offset used, shift = 0 corresponds to an abscissa value of 51.

7. The steps 4 through 6 are repeated till all 128 range intervals have been processed. To the observed data kmax(i), a linear function a + b i is fitted. In the ideal case, perfect focussing occurs when kmax ≈ 0, a = 0 , b = 0. In the beginning of the iteration procedure, in general, a and b will substantially deviate from zero. The determined values then are used to compute new processor constants A and B to be used in $f_{rP}(i) = A + B i$, and a next iteration is started. Figure 1.14 shows lag lines observed for different processor Doppler frequency functions, the top and bottom functions correspond with heavily defocussed images, the middle one corresponds with the focussed images. The iteration procedure comes to an end when the stop criterion $\sum_{i=1}^{128} kmax(i)^2 < \varepsilon$ is met. The corresponding processor values, A and B, are the best estimates of the Doppler rate line $f_{DR}(i) = A + B i$. The lag estimation error decreases when the width of the cross-correlation function decreases. A sharp peak will give smaller errors than a wide one. Thus, the error is not only related to the signal-to-noise ratio, but also to the scene characteristics. The autofocus technique is most accurate for a scene that exhibits bright point targets and is significantly degraded for ocean or desert. The scenes with relatively few bright targets will show broader cross-correlation peaks and therefore have a higher degree of uncertainty for the Doppler frequency rate estimate.

In [Li 85] test results are shown for the autofocus technique for the Goldstone tracking station scene, an agricultural field pattern and a patch of ocean in the Bay area. The rms deviations are ≈ 0.1 Hz/sec for the Goldstone scene and 0.2 Hz/sec for the agricultural scene. The increased deviation in case of the agricultural scene is attributed to the lack of bright point like targets in the scene. Visual examination of the ocean image revealed no sharp boundaries or point-like features, and, no consistent trend in the observed maxima was found. They concluded that the autofocus method cannot be applied to this type of scene. For most images over land, however, they believed that this method should be effective.

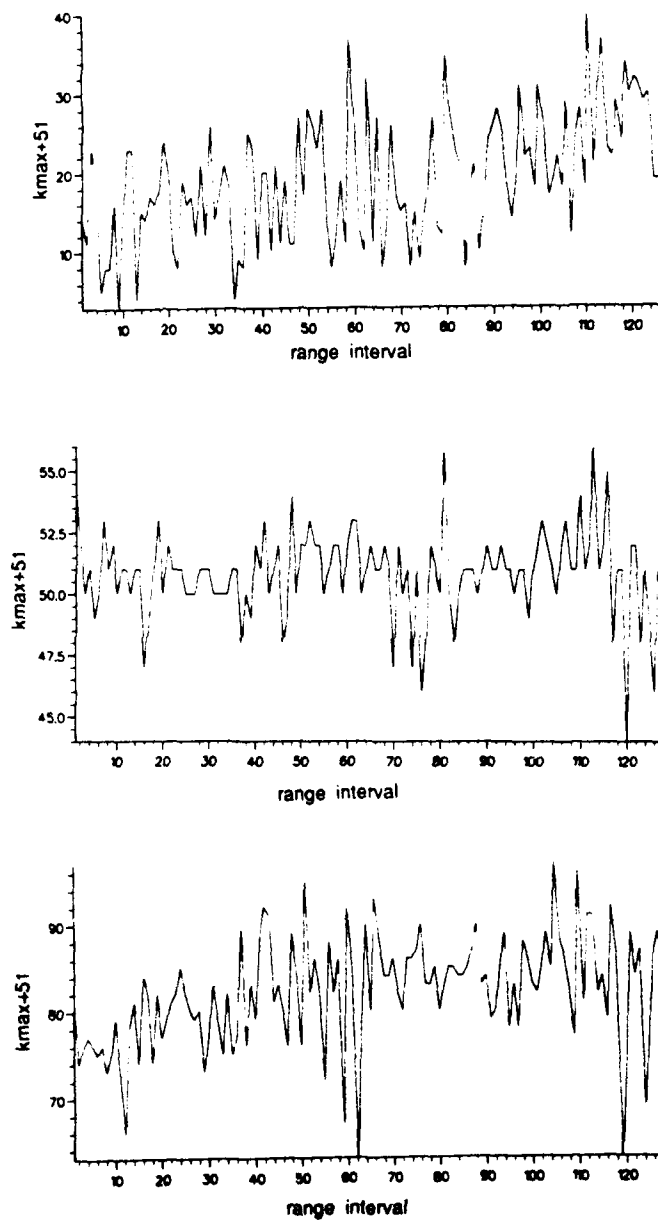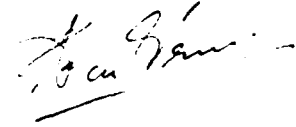The rms deviation of our processing result was 0.04 Hz/sec.

Figure 1.14: Observed lag lines for different processor Doppler frequency functions $f_m(i) = A + B \, i$. From top to bottom A=506 , B=0 ; A=518 , B=-0.03 uniformly focussed; A=526 , B=0.

REFERENCES

[Otten 89] M.P.G.Otten ,"Phase error estimation for PHARUS: a review of autofocus and related
algorithms", FEL-TNO report FEL-89-C243,Sept.,1989

[Brown 88] W.D.Brown and D.C.Ghiglia, "Some methods for reducing propagation-induced
phase errors in coherent imaging systems. I Formalism", J.Opt.Soc.Am.
A/Vol.5,No.6/June 1988.

[Li 85] F.Li, D.N.Held, J.C.Curlander and C Wu ,"Doppler Parameter Estimation for Spaceborne
Synthetic-Aperture Radars", IEEE Transactions Geoscience and Remote
Sensing,Vol.GE-23,No.1,Januari 1985

[Madsen 89] S.N.Madsen, "Estimation The Doppler Centroid of SAR Data", IEEE Transactions
on Aerospace and Electronic Systems Vol.AES-25,No2, March 1989

[Barber 85] B.C.Barber ,"Theory of digital imaging from orbital synthetic-aperture radar", Int.
J.Remote Sensing, 1985, Vol.6, No.7, p1009-1057

[Curlander 82] J.C.Curlander, C.Wu, A.Pang, "Automatic Preprocessing of Spaceborne SAR
Data", In Proceedings of the 1982 International Geoscience and Remote Sensing
Symposium, Munich, W. Germany, June 1982, pp.3.1-3.6

[Tomiyasu 80] K.Tomiyasu ,"Tutorial review of synthetic aperture radar (SAR) with applications
to imaging of the ocean surface", Proc. IEEE, vol. AES-18, pp 563-575, May 1980

[Madsen 86] S.N.Madsen, "Speckle theory, modelling, analysis and applications related to
synthetic aperture radar data." Ph.D thesis (report LD62),Electro-magnetics Institute,
Lyngby, Denmark, Nov.1986

F.P.Ph. de Vries

(Group leader)   (Author)

A.1   RANGE-AZIMUTH SHIFT INDUCED BY AN INCORRECT DOPPLER
CENTROID VALUE OF THE PROCESSOR.

Figure A.1 shows the position of the point target locus, $t = 0$ corresponds with the moment where
the target is in the antenna boresight direction. Also shown is the reference locus with centre
(τ, ρ).

At the time τ an image point (in general not the image point of the point target) is computed by
the azimuth compression.

The correlator output due to the point target is

$$C(\tau) = \int_{-T_a/2}^{T_a/2} s_t(\tau + \beta)s_r^*(\beta)d\beta \qquad (A.1)$$

where T_a is the azimuth integration time, $s_r(\beta)$ the azimuth reference function and $s_t(\tau + \beta)$ the
point target signal encountered along the reference locus. If the processor uses the correct Doppler
parameters, the Doppler centroid value f_{DC} and Doppler rate f_{DR}, the maximum point target
output occurs at $\tau = 0$ (and $\rho = 0$). If incorrect processor parameter values are used, the maximum
point target response will occur at a value of $\tau \neq 0$ (and $\rho \neq 0$). The value of τ and ρ as a function
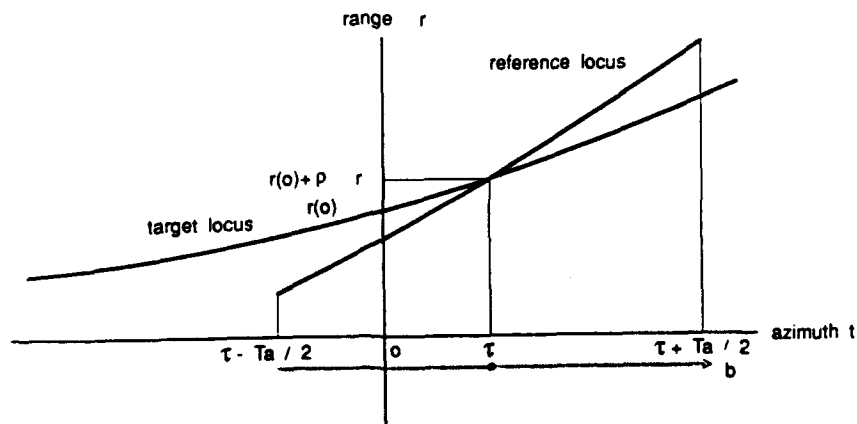

Figure A.1:   Position of reference and target locus.

of parameter mismatch is derived below.

The target locus is

$$r_t(t) = a_{0t} + a_{1t}t + a_{2t}t^2 \tag{A.2}$$

The reference locus is

$$r_r(\beta) = r_t(\tau) + a_{1r}\beta + a_{2r}\beta^2 \tag{A.3}$$

For the difference between target and reference locus we find

$$\delta_r(\beta) = r_t(\tau + \beta) - r_r(\beta) = r_t(\tau + \beta) - r_t(\tau) - (a_{1r}\beta + a_{2r}\beta^2) \tag{A.4}$$

From A.2 it follows

$$r_t(\tau + \beta) = r_t(\tau) + (a_{1t} + 2a_{2t}\tau)\beta + a_{2t}\beta^2 \tag{A.5}$$

Substitution of A.5 into A.4 gives

$$\delta_r(\beta) = (a_{1t} + 2a_{2t}\tau)\beta + a_{2t}\beta^2 - (a_{1r}\beta + a_{2r}\beta^2) \tag{A.6}$$

Assuming a correct processor value for a_2 we have

$$a_{2r} = a_{2t} \tag{A.7}$$

hence

$$\delta_r(\beta) = \{(a_{1t} + 2a_{2t}\tau) - a_{1r}\}\beta \tag{A.8}$$

We see that the loci coincide for

$$\tau_o = \frac{a_{1r} - a_{1t}}{2a_{2t}} \tag{A.9}$$

With

$$s_t(\alpha) = a(\alpha)\exp j\phi_t(\alpha)$$

where $a(\alpha)$ is caused by the antenna and

$$s_r(\beta) = \exp j\phi_r(\beta)$$

with
$$\phi_t(\alpha) = c_{0t} + c_{1t}\alpha + c_{2t}\alpha^2$$
$$\phi_r(\beta) = c_{0r} + c_{1r}\beta + c_{2r}\beta^2$$

we find

$$C(\tau) = \exp j(c_{0t} + c_{1t}\tau + c_{2t}\tau^2 - c_{0r})$$

$$\times \int_{-T_a/2}^{T_a/2} a(\tau + \beta) \exp j[(c_{1t} + 2c_{2t}\tau - c_{1r})\beta + (c_{2t} - c_{2r})\beta^2]d\beta \qquad (A.10)$$

from 1.7, .29 and .31

$$\tau_0 = \frac{c_{1r} - c_{1t}}{2c_{2t}}$$

$$c_{2r} = c_{2t}$$

it follows

$$C(\tau_0) = \exp j\{\phi_t(\tau_0) - c_{0r}\} \int_{-T_a/2}^{T_a/2} a(\tau_0 + \beta)d\beta \qquad (A.11)$$

Thus the coincidence of the target- and reference locus yields an "inphase" integration and thus the maximum output.

Note 1: We tacitly assume the "inphase" integration to be far more important than a value of τ smaller than τ_0. It is true that

$$\int_{-T_a/2}^{T_a/2} a(\tau + \beta)d\beta < \int_{-T_a/2}^{T_a/2} a(\tau_o + \beta)d\beta$$

when

$$\tau < \tau_0$$

but since the reference locus and the target locus do not coincide, a phase function occurs and the signal amplitude along the reference locus is not coherently added.

$$|C(\tau)| = |\int_{-T_a/2}^{T_a/2} \exp j[\varepsilon(\tau)\beta]a(\tau + \beta)d\beta| < \int_{-T_a/2}^{T_a/2} a(\tau_0 + \beta)d\beta)|$$

Note 2: From the form of the antenna pattern and .33 follows

$$|C(\tau_0)| < \int_{-T_a/2}^{T_a/2} a(\beta)d\beta \qquad (A.12)$$

so due to the incorrect a_{1r} value used we lose signal energy.

The range offset value ρ which corresponds to τ_0 is

Appendix A

$$\rho = r(\tau_0) - r(0) = a_{1t}\tau_0 + a_{2t}\tau_0^2$$

$$\rho = \frac{a_{1r} + a_{1t}}{2}\tau_0 = \frac{a_{1r} + a_{1t}}{2}\frac{a_{1r} - a_{1t}}{2a_{2t}} = \frac{a_{1r}^2 - a_{1t}^2}{4a_{2t}} \qquad (A.13)$$

Using 1.8 and 1.9 we can write A.9 and A.11 as

$$\tau_0 = \frac{1}{f_{DR}}(f_{DP} - f_{DC}) \qquad (A.14)$$

$$\rho = \frac{-\lambda}{2f_{DR}}(\frac{f_{DP} + f_{DC}}{2})(f_{DP} - f_{DC}) \qquad (A.15)$$

REPORT DOCUMENTATION PAGE (MOD-NL)

1. DEFENSE REPORT NUMBER (MOD-NL) TD91-3978	2. RECIPIENT'S ACCESSION NUMBER	3. PERFORMING ORGANIZATION REPORT NUMBER FEL-91-B331
4. PROJECT/TASK/WORK UNIT NO. 22020	5. CONTRACT NUMBER -	6. REPORT DATE NOVEMBER 1991
7. NUMBER OF PAGES 39 (INCL APPENDIX, EXCL. RDP & DISTRIBUTION LIST)	8. NUMBER OF REFERENCES 8	9. TYPE OF REPORT AND DATES COVERED FINAL

10. TITLE AND SUBTITLE
ESTIMATION OF THE PARAMETERS USED IN THE AZIMUTH COMPRESSION

11. AUTHOR(S)
F.P.PH. DE VRIES

12. PERFORMING ORGANIZATION NAME(S) AND ADDRESS(ES)
TNO PHYSICS AND ELECTRONICS LABORATORY, P.O. BOX 96864, 2509 JG THE HAGUE
OUDE WAALSDORPERWEG 63, THE HAGUE, THE NETHERLANDS

13. SPONSORING/MONITORING AGENCY NAME(S)
NETHERLANDS AGENCY FOR AEROSPACE PROGRAMS (NIVR)

14. SUPPLEMENTARY NOTES

15. ABSTRACT (MAXIMUM 200 WORDS, 1044 POSITIONS)
IN AZIMUTH PROCESSING OF SAR DATA, THE SLANT RANGE HISTORIES OF THE TARGETS ARE REQUIRED. AFTER RANGE COMPRESSION THE MAXIMA OF THE RESPONSES OF A POINT TARGET ARE ON THE SO CALLED RANGE MIGRATION LOCUS. FOR SPACEBORNE SAR THE LOCUS TRAVERSES A NUMBER OF RANGE BINS. THIS LOCUS DETERMINES WHERE TO GET THE SAMPLES NEEDED FOR THE AZIMUTH COMPRESSION AND THE PHASE FUNCTION WHICH MUST BE USED. FOR SATELLITE SAR THE LOCUS CAN BE DESCRIBED BY TWO PARAMETERS, THE DOPPLER CENTROID f_{DC} AND THE FREQUENCY RATE f_{DR}. THESE PARAMETERS CAN BE ESTIMATED BY USING ACCURATE SPACECRAFT ANCILLARY DATA AND BY UTILIZING THE RECEIVED RADAR DATA ALONE. THIS REPORT DESCRIBES THE EFFECTS OF ERRORS IN THE PARAMETERS USED BY THE PROCESSOR AND DISCUSSES ALGORITHMS TO ESTIMATE THE PARAMETERS. EXAMPLES OF RESULTS FROM PROCESSING SEASAT DATA ARE SHOWN.
THE REPORT IS ONE OF A SERIES FOR A SAR PROCESSOR FOR THE ERS-1 DATA, PHASE 2, PRECISION PROCESSOR. THE WORK DESCRIBED WAS SUBSIDIZED BY THE NIVR (NIVR, NRT NR, 2802 FE, SAR PROCESSOR).

16. DESCRIPTORS	IDENTIFIERS
SYNTHETIC APERTURE RADAR SATELLITE BORNE ESTIMATION	DIGITAL SIGNAL PROCESSOR DOPPLER PARAMETERS DOPPLER CENTROID DOPPLER FREQUENCY RATE

17a. SECURITY CLASSIFICATION (OF REPORT) UNCLASSIFIED	17b. SECURITY CLASSIFICATION (OF PAGE) UNCLASSIFIED	17c. SECURITY CLASSIFICATION (OF ABSTRACT) UNCLASSIFIED
18. DISTRIBUTION/AVAILABILITY STATEMENT UNLIMITED		17d. SECURITY CLASSIFICATION (OF TITLES) UNCLASSIFIED